ELSEVIER

Contents lists available at ScienceDirect

Minerals Engineering

journal homepage: www.elsevier.com/locate/mineng





Starch adsorption on hematite surfaces: Evidence of the adsorption mechanism dependence on the surface orientation

Lizbet León Félix ^{a,b}, Gabriela F. Moreira ^{a,b}, Laurindo S. Leal Filho ^{a,c}, Fernando Stavale ^{b,*}

- ^a Instituto Tecnológico Vale ITV, Avenida Juscelino Kubitschek, 31, Ouro Preto, MG 35.400-000, Brazil
- ^b Centro Brasileiro de Pesquisas Físicas CBPF/MCTI, Rua Xavier Sigaud 150, Rio de Janeiro, RJ 22290-180, Brazil
- ^c Laboratory of Transport Phenomena and Chemistry of Interfaces, Department of Mining and Petroleum Engineering, Av. Prof. Mello Moraes 2237, University of São Paulo. São Paulo. Brazil

ABSTRACT

In this study, the adsorption mechanism of amylopectin molecules on the hematite (1 1 $\overline{2}$ 0), (1 $\overline{1}$ 0 0) and (0 0 0 1) single-crystal surfaces were investigated by surface-sensitive techniques. Our results show evidence of preferential adsorption on the hematite surface planes in the order of (1 1 $\overline{2}$ 0) > (1 $\overline{1}$ 0 0) > (0 0 0 1). Based on these findings, we propose that distinct singly and triply coordinated oxygen atoms on the surface react in pairs by a multisite complexation mechanism to promote the attachment of amylopectin molecules. These results demonstrate the pivotal role of the exposed hematite surface structure–reactivity relationship in starch adsorption and the possible causes of inefficiencies in industrial flotation processes, as well as biomedical and environmentally friendly technologies based on hematite nanoparticles.

1. Introduction

Hematite (α-Fe₂O₃) has been widely explored in various fields for use in heterogeneous catalysts (Pham et al., 2009), in biomedical applications Figuerola et al. (2010) or as an electrode material for light-driven water splitting reactions (Kim, 2013; Chatman et al., 2015). Its chemical and physical properties depend on the exposed particle surface planes, since a particular surface structure may govern the interaction between oxide and environmental conditions and, consequently, the material functionalities (Patra et al., 2016; Stumm, 1992). A technological example of the interplay between the surface structure and chemical reactivity of hematite is found in the reverse flotation of iron ores in basic medium (Filippov et al., 2014). Following this particular industrial application, after comminution and sizing, the aqueous slurry composed mainly of particles of hematite and quartz is conditioned with starch, which selectively adsorbs onto hematite particles, reinforcing its natural hydrophilic character and preventing the nonspecific adsorption of other hydrophobic reagents. Conversely, the addition of long-chain cationic surfactants to the slurry allows their adsorption onto quartz, making the surface of the particles hydrophobic. Because waterrepellent quartz particles are likely to attach to air bubbles and float, whereas hydrophilic particles of hematite tend to sink, starch is regarded as a depressant agent. Previous reports in the literature have described the dependence of crystallographic surface orientation molecule adsorption on hematite surfaces (Taylor et al., 2019; Yan et al., 2020). Therefore, one may expect that the mineral concentration process described above is likely to be affected by the interaction of starch molecules on specific hematite particle facets, that is, related to the iron ore mineralogy (Leal Filho et al., 2000; Shrimali, 2018; Mhonde et al., 2017)

The fundamental mechanism that describes the starch adsorption on hematite surfaces is also connected to the chemistry of the starch molecules in solution. Starch is a complex natural polymer consisting of two fractions: $\sim 20\text{--}25\%$ is amylose, and $\sim\!\!75\text{--}80\%$ is amylopectin. For instance, amylopectin molecules are known to act as a better depressor than amylose molecules (Mhonde et al., 2017; Araujo et al., 2005), although the exact mechanism of the adsorption interaction remains unclear (Xia et al., 2009; Liu et al., 2000). The general understanding is that this interaction occurs initially through the-OH functional groups of the starch molecule and the oxy/hydroxyl groups on the hydroxylated iron surface atoms (Shrimali, 2018; Mhonde et al., 2017; Turrer and Peres, 2010; Weissenborn et al., 1995). Next, chemical forces appear to govern the interaction between the acidic ferric iron surface atoms on hematite and the-OH functional groups on the starch molecule, leading to chemical complexation (Pavlovic and Brandao, 2003; Laskowski et al., 2007; Ravishankar et al., 1995). In addition to the -OH functional groups, the carboxylate groups in the molecule may contribute to the strength of the acid/base interaction (Moreira et al., 2017; Tang and Liu,

E-mail address: stavale@cbpf.br (F. Stavale).

 $^{^{\}ast}$ Corresponding author.

2012). Importantly, if the acid/base interaction model holds, starch adsorption will critically depend on the bond valence and coordination of the iron surface atoms and, therefore, on the hematite surface structure.

Despite these efforts to understand the mechanism of the interaction between starch and iron oxides, to the best of our knowledge, investigations of the role of metal-hydroxyl species on the hematite surface orientation are still lacking. Hence, detailed studies on well-defined single crystal surfaces may provide relevant information about their surface structure—reactivity relationship towards starch adsorption. This is particularly important because upon formation of hydroxyl groups on the oxide surface by dissociative adsorption of water, chemically reactive sites (Cornell and Schwertmann, 2004) may control the spatial distributions of adsorbed molecules (Hiemstra and Van Riemsdijk, 1999; Barrón and Torrent, 1996; Venema et al., 1998; Hiemstra et al., 1989).

To gain insight into this starch adsorption behavior, we investigated amylopectin molecules adsorbed on the well-defined surfaces of hematite single crystals by means of (near-)surface sensitive techniques (attenuated total reflection Fourier transform infrared (ATR-FTIR), atomic force microscopy (AFM) and X-ray photoelectron spectroscopy (XPS)). The selected hematite surface orientations were the natural (1 1 $\overline{2}$ 0), (1 $\overline{1}$ 0 0) and (0 0 0 1) α -Fe₂O₃ single crystal surfaces due to their differences in surface structure and density of chemical species. Moreover, distinct hydroxyls and low-coordinate surface atoms are expected to play a pivotal role in the surface reactivity and starch adsorption affinity. As a consequence, our results show evidence of a multisite complexation mechanism in which both singly and triply coordinated oxygen surface atoms react in pairs to achieve attachment of amylopectin molecules. Furthermore, the mechanism must be rationalized not only based on the surface density of singly coordinated oxygen atoms but also in terms of the actual density of reactive iron sites on the surface.

2. Experimental methods

2.1. Materials

The high-grade corn starch employed in this study is composed of 95% amylopectin (Fluidex SS-22 from Ingredion Ltda) and analytical sodium hydroxide (Vetec Ltda). Natural hematite $(\alpha\text{-Fe}_2O_3)$ single crystals were used in the following crystallographic orientations: (1 1 $\overline{2}$ 0), (1 $\overline{1}$ 0 0) and (0 0 0 1). The (0 0 0 1) single crystal was obtained from Minas Gerais State, Brazil, and the other two were purchased from MTI Corporation. Solutions of H_2SO_4 and NaOH were used to adjust the pH value, and ultrapure deionized water was used in all experiments.

2.2. Preparation of α -Fe₂O₃ single crystal surfaces

All hematite single crystals were repolished, and their orientation was confirmed by electron backscatter diffraction (EBSD) (JSM-7100F from JEOL). The EBSD patterns obtained for each crystal are shown in supporting material Fig. S1. Next, all hematite pristine surfaces were prepared by several cycles of thermal treatments at 700 $^{\circ}$ C for 12 h in pure synthetic air flow and manual polishing to remove hydroxyl species and organic contaminants as well as metallic impurities from their surface. Pristine hematite surface flatness and cleanness were verified by surface sensitive AFM (supporting material Fig. S2a) and XPS measurements.

2.3. Hydroxylation and starch adsorption conditions

For surface hydroxylation experiments, crystals were conditioned in an aqueous solution at pH 10 under constant stirring at 100 rpm in an orbital shaker for 150 min at room temperature. Gelatinized starch was

prepared by adding NaOH (10% w/v) to an aqueous starch solution under vigorous stirring. The starch:NaOH ratio used was 5:1, and the solution was later diluted in deionized water to achieve the desired concentration. Next, adsorption of 50 mg/L and 100 mg/L starch was performed on each crystallographic orientation with an adjusted pH of 10, as indicated in the text. The single crystals were conditioned in starch solution under continuous agitation at 100 rpm in an orbital shaker at room temperature for 30 min. Afterward, the crystals were repeatedly washed with deionized water to remove the non-adsorbed starch and dried with a high-purity N2 gas flow. The pH 10 conditioning was used because starch is mostly used in industrial flotation processes in alkali aqueous solutions, which display the best depression performance at approximately pH 10-10.5. The adsorption tests were performed using a low concentration of starch to qualitatively determine the AFM starch relative coverage on the hematite as a function of the concentration. During the experiments, sample conditioning at starch concentration above 100 mg/L made a thick starch film form, where the adsorption mechanism was not identifiable. After starch conditioning, all hematite surfaces were cleaned by several cycles in ultrasonic water bath at 40–60 °C (supporting material Fig. S2b).

2.4. Atomic force microscopy (AFM)

AFM was used to evaluate the surface topography and the number of adsorbed species on each crystallographic surface plane. The AFM experiments were carried out on a Nanoscope V (MultiMode 8) at room temperature. The samples were examined by tapping mode AFM with standard silicon nitride cantilever tips with a resonant frequency between 90 and 240 kHz, a tip radius of less than 10 nm and a force constant of approximately $0.08\ Nm^{-1}$. The scan rate was typically $1.0\ Hz$, and the data collection was 512 lines per sample. The root-mean-square (rms) surface roughness values were obtained in different regions and averaged between 9 images with a scan size of 5 $\mu m \times 5 \ \mu m$ for all surfaces; the results were processed using Nanoscope software (V1.5).

2.5. X-ray photoelectron spectroscopy (XPS)

The surface chemical composition was investigated by highresolution X-ray photoelectron spectroscopy using a SPECS GmbH system (with a base pressure greater than 10⁻⁹ mbar) equipped with a PROIBOS 150 hemispherical electron analyzer with a monochromatic Al-Kα radiation source. The spectra were recorded with a pass energy of 50 or 15 eV for surveys and high-resolution measurements, respectively. The spectrometer was previously calibrated using the Au $4f^{7/2}$ core level, resulting in a FWHM of 0.7 eV for a sputtered metallic gold foil. All pristine crystals showed relatively large amounts of adventitious carbon, but the samples were not sputtered, since preferential sputtering of oxygen over iron is known to reduce oxidation of the original surface. The spectra binding energies were recalibrated due to charging effects for each surface investigated by setting the Fe 3p core level to 56 eV. The fitting procedure was performed using CasaXPS software. Spectral analysis was performed by fitting the peak envelope using Gaussian/ Lorentzian functions and Shirley-type background for all peak regions. The estimated quantification of the C 1s increase for a given surface plane was calculated from the survey spectra peak areas of C 1s and Fe 2p in the binding energy interval from 292 to 280 eV and from 738 to 705 eV, respectively. The calculated carbon increases after the starch adsorption with respect the corresponding hydroxylated surface were 9, 5.5 and 3.3 times larger for $(1\ 1\ \overline{2}\ 0)$, $(1\ \overline{1}\ 0\ 0)$ and $(0\ 0\ 0\ 1)$, respectively. To directly compare the carbon amount adsorbed on each surface plane, we normalized the largest increase (for the $(1\ 1\ \overline{2}\ 0)$ orientation) as 1. All measurements were performed on freshly prepared samples after air-to-ultrahigh vacuum transfer to guarantee the reproducibility of the results.

2.6. Attenuated total reflection Fourier transform infrared (ATR-FTIR)

ATR measurements were performed by a vacuum Fourier transform infrared (FTIR) spectrometer (VERTEX 70v from Bruker) equipped with a diamond crystal ATR accessory (Platinum ATR). The instrument was equipped with a DLaTGS detector with a KBr window that covers a spectral range from 8000 to 250 cm $^{-1}$. ATR-FTIR spectra were obtained in the spectral range of 4500–330 cm $^{-1}$; 64 scans at 4 cm $^{-1}$ per spectrum were obtained and analyzed using OPUS version 8.1 software. All spectra were obtained at 25.9 °C and 1% relative humidity. The spectra were recorded by contacting the ATR crystal directly onto the surfaces.

3. Results and discussion

3.1. Atomic force microscopy analysis

To identify the possible effects of surface hydroxylation, since

morphological changes would affect the adsorption of molecules, we investigated the difference in roughness between the pristine surface and the surface treated at pH 10. AFM measurements (supporting material Fig. S2) of the surface topography of the pristine (1 1 $\overline{2}$ 0), (1 $\overline{1}$ 0 0) and (0 0 0 1) surfaces indicated RMS roughness values of 0.14 \pm 0.02, 0.26 \pm 0.05 and 0.20 \pm 0.06 nm, in contrast to the surfaces after hydroxylation, which had values of 0.18 \pm 0.03, 0.27 \pm 0.08 and 0.23 \pm 0.03 nm, respectively. Apparently, the hydroxylation treatment did not lead to a drastic modification of the surface roughness, and the expected changes were mostly chemical changes related to the attachment of hydroxyl groups.

Figs. 1 and 2 show AFM topographic images demonstrating the effects of 50 mg/L and 100 mg/L starch adsorption, respectively, on hydroxylated hematite surfaces with different orientations. As expected, the amount of adsorbed starch on the surface increased as a function of starch concentration. Fig. 1 depicts AFM images after adsorption of 50 mg/L starch on each surface, with image sizes of 2×2 µm and 500×10^{-2}

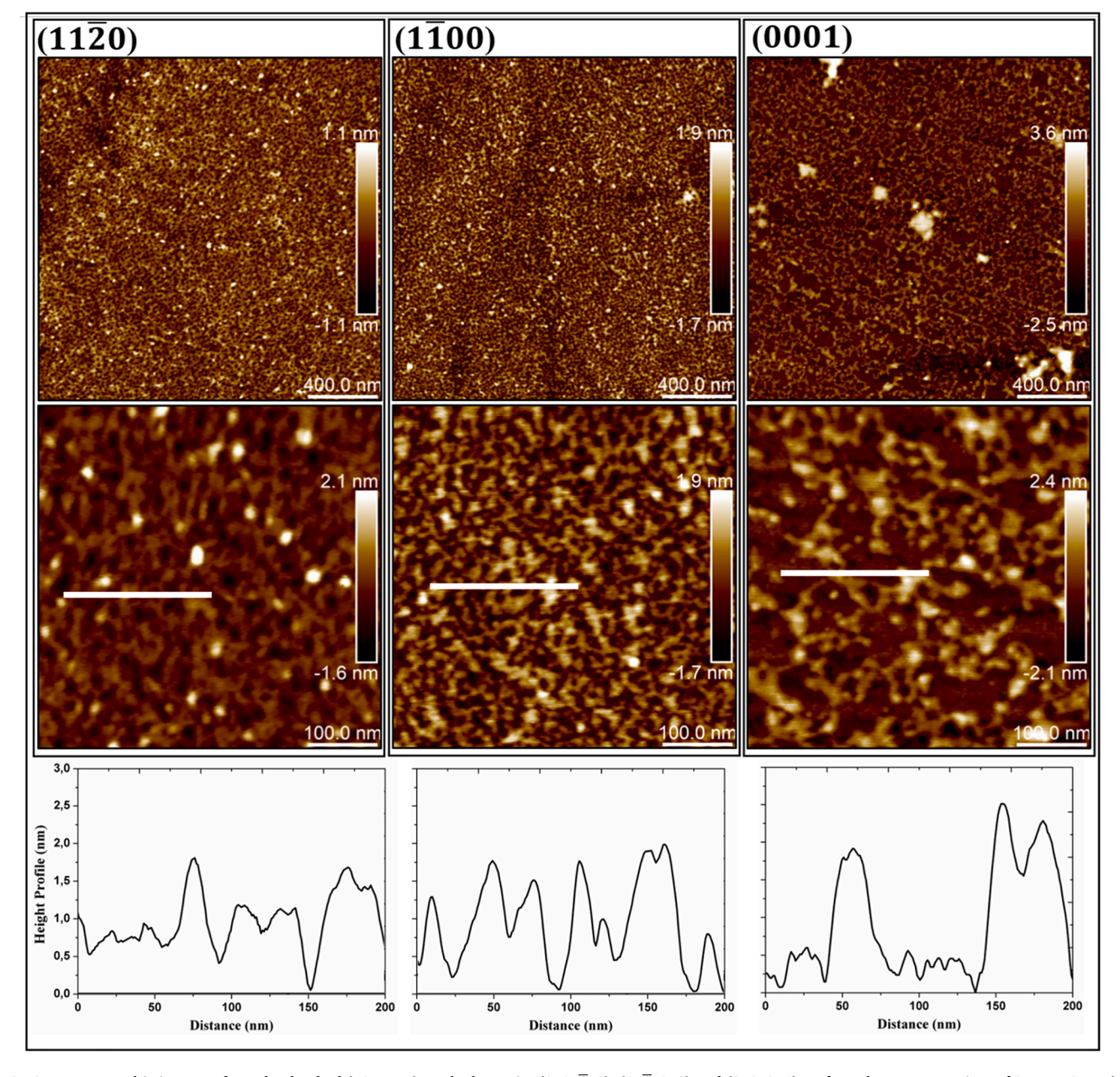


Fig. 1. AFM topographic images of starch adsorbed (50 mg/L) on the hematite (1 $1\ \overline{2}$ 0), (1 $\overline{1}$ 0 0) and (0 0 0 1) surface planes. Image sizes of 2 μ m \times 2 μ m (top) and 500 nm \times 500 nm (bottom). Bottom panel: height profiles at the positions indicated by the continuous white lines in the topographic images.

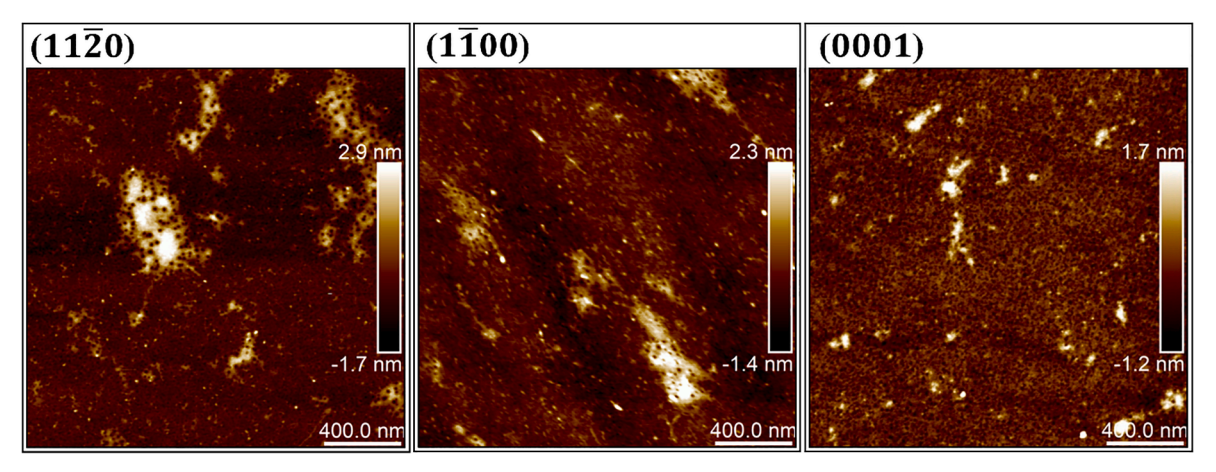


Fig. 2. AFM topographic images of starch adsorbed (using 100 mg/L) on the hematite (1 1 $\overline{2}$ 0), (1 $\overline{1}$ 0 0) and (0 0 0 1) surface planes. Image size of 2 μ m \times 2 μ m.

500 nm, allowing comparison between the orientations. The surface consisted of a film and small aggregates dispersed on all the surfaces. We note, however, a highly homogeneous surface coverage for the $(1\ 1\ \overline{2}\ 0)$ and $(1\ \overline{1}\ 0\ 0)$ surfaces compared to the $(0\ 0\ 0\ 1)$ orientation. In Fig. 1, close inspection of the (0 0 0 1) surface reveals several open patches exposing the surface underneath. This heterogeneous film formation reveals, on the one hand, a weaker adsorption affinity toward starch in this particular orientation. On the other hand, the starch-starch interaction prevails and results in the formation of islands, which can be seen in the larger image depicted in Fig. 1. These morphological changes promoted by few-layer starch adsorption can be observed using surface height profiles in Fig. 1 lower panel, which were obtained at the positions marked by the white line in the images. The apparent height from the bottom of the open patches to the island top is approximately 2 nm, which corresponds to the first layer of starch; in contrast, the small, dispersed aggregates had heights of ~5 nm. A comparison between the hydroxylated surface and the starch-adsorbed surface also indicates differences in the adsorption behavior. We noted that after starch adsorption, the surface roughness of the $(1 \ 1 \ \overline{2} \ 0)$, $(1 \ \overline{1} \ 0 \ 0)$ and (0 0 0 1) surfaces increased to 0.26 \pm 0.14, 0.49 \pm 0.03 and 0.42 \pm 0.12 nm, respectively. We explain these differences by the fact that on the $(1\ 1\ \overline{2}\ 0)$ surface, the stronger starch-hematite interaction promotes a sort of two-dimensional growth, resulting in a smaller overall roughness than that of the other two orientations investigated.

Fig. 2 shows AFM images of 100 mg/L starch adsorbed on hematite. As in the sample with 50 mg/L starch, an interconnected network structure is attached to the surface and decorated by large aggregates dispersed on all orientations. We note, however, that larger nonuniform agglomerates are present on the surface, particularly on the $(1 \ 1 \ \overline{2} \ 0)$ and $(1 \ \overline{1} \ 0 \ 0)$ surface planes. An increase in starch concentration resulted in a homogeneous starch film and many nonuniform agglomerates covering the hematite surfaces. This behavior can be clearly seen by comparing the images in Fig. 1 and Fig. 2. The height of these large aggregates was estimated to be \sim 5 nm, which is within the same height range observed for the samples prepared with 50 mg/L starch. These results indicate that the starch concentration significantly affects the amount of starch adsorbed. Notably, the starch interaction is stronger for the $(1 \ 1 \ \overline{2} \ 0)$ and $(1 \ \overline{1} \ 0 \ 0)$ surfaces than for the $(0 \ 0 \ 0 \ 1)$ surface. These differences are also observed when one compares the roughness under these conditions, with values of 0.80 \pm 0.11, 0.98 \pm 0.08 and 0.51 \pm 0.20 nm for the (1 1 $\overline{2}$ 0), (1 $\overline{1}$ 0 0) and (0 0 0 1) surfaces, respectively. To support this preferential adsorption, we have also analyzed the average coverage obtained with 50 mg/L starch conditioning (supporting material Fig. S3). The starch area occupation for each surface plane is $\sim 60\%$, $\sim 50\%$ and $\sim 40\%$ for the (1 1 $\overline{2}$ 0),

 $(1 \ \overline{1} \ 0 \ 0)$ and $(0 \ 0 \ 0 \ 1)$ surfaces, respectively.

3.2. ATR-FTIR measurements

Additional information about the chemical modifications promoted on all pristine surfaces after hydroxylation was obtained from ATR-FTIR spectroscopy. Fig. 3a shows the ATR-FTIR spectra of all surfaces before and after hydroxylation. The hematite space group and atomic positions indicate the number, type and symmetry of the vibrational modes in the infrared spectra, as extensively discussed in the literature (Fateley et al., 1971; Hofmeister, 1993; Rendon and Serna, 1981; Onari et al., 1977; Wang et al., 1998). Two A_{2u} and four E_u (and their corresponding traversal and longitudinal) asymmetrical modes related to Fe-O vibrations were expected. These modes correspond to dipolar transitions parallel (A_{2u}) and perpendicular (E_u) to the $[0\ 0\ 0\ 1]$ crystal direction. Thus, in Fig. 3a, the most intense bands were observed at approximately 375-381 (E_u), 420-450 (E_u), 502-504 (E_u) and 565-700 (A_{2u}) cm⁻¹ There are, however, subtle but significant spectral differences between each surface orientation. First, despite the distinct crystal orientations, similar spectral features are related to the shared bulk Fe-O6 and O-Fe4 octahedral and tetrahedral sites, respectively. Second, the differences in the band intensity are connected to the fact that for each surface orientation, the light incidence in the ATR accessory with respect to the [0 0 0 1] crystal direction is modified.

In Fig. 3a, we note several modifications after surface hydroxylation on all surfaces. The spectral changes correspond to the conversion of the oxide surface into a goethite-like surface (Morterra et al., 1984; Farmer, 1968; Verdonck et al., 1982; Cambier, 1986). One can observe an enhancement of the bands near 565-700 cm⁻¹ attributed to Fe—O stretching vibrations in goethite (Prasad et al., 2006; Ruan et al., 2001; Gotić and Musić, 2007). The band located at 630 cm⁻¹ was previously reported to be related to hydroxyl groups (Cambier, 1986; Prasad et al., 2006) in hydrohematite (Ruan et al., 2001; Chernyshova et al., 2007) and to the out-of-plane Fe-OH vibrations in goethite. Likewise, other reports have assigned the band near 603–618 cm⁻¹ as a characteristic band of goethite samples (Ruan et al., 2001; Humez and Prost, 1999; Silva et al., 2006). Particularly interesting, however, is the new band detected near 565 cm⁻¹ on all surfaces after the hydroxylation treatment. This band appears to be related to OH groups, as previously reported for Fe(III)hydroxides (Verdonck et al., 1982; Fischer and Schwertmann, 1975). This result reveals that after hydroxylation, all pristine surfaces display considerable chemical changes, as OH groups are attached to the surface. Notably, the hydroxylation process of the $(1 \ 1 \ \overline{2} \ 0)$ surface appears to differ slightly from that observed for the $(1 \ \overline{1} \ 0 \ 0)$ and $(0 \ 0 \ 1)$ orientations. In Fig. 3a, a new relatively broad band at 450 cm⁻¹ is identified. This new band might be related to

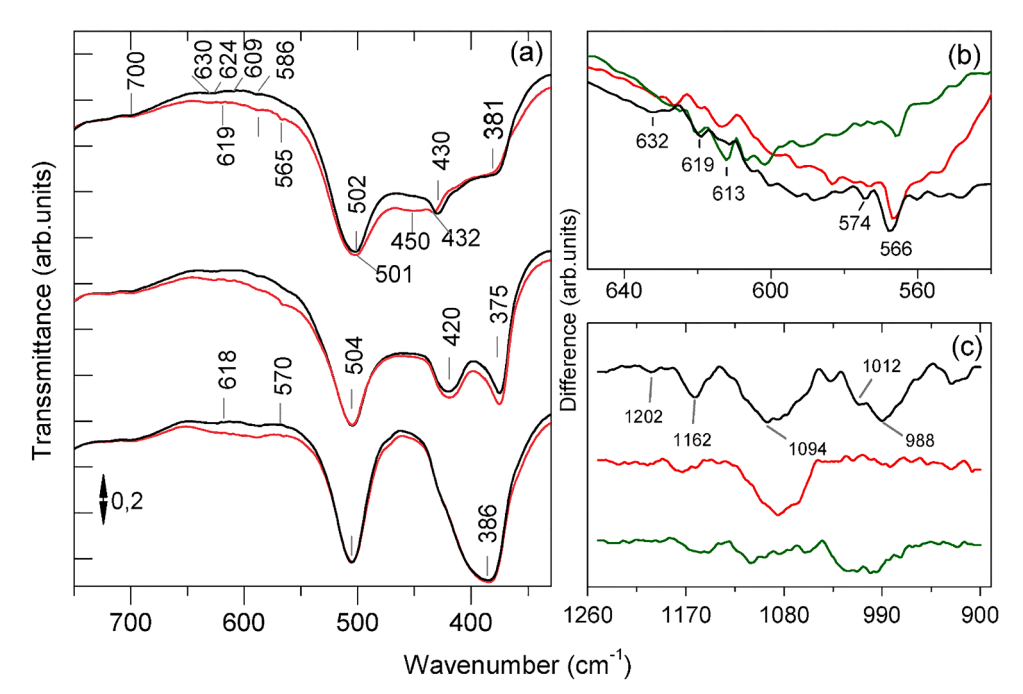


Fig. 3. ATR-FTIR spectra of hematite in the (a) (1 1 $\overline{2}$ 0), (1 $\overline{1}$ 0 0) and (0 0 0 1) surface planes before (black line) and after (red line) hydroxylation, (b) ATR-FTIR difference spectra of the hydroxylated with respect the pristine hematite surface and (c) ATR-FTIR difference spectra after the starch adsorption with respect the hydroxylated hematite surface. The spectra are shifted in the vertical axis for clarity. (For interpretation of the references to colour in this figure legend, the reader is referred to the web version of this article.)

hydroxyl groups attached to low-symmetry three-coordinate oxygen sites (OFe₃) on the (1 1 $\overline{2}$ 0) surface, as reported previously for α -FeOOH (Verdonck et al., 1982). This increase of the hydroxyls related bands can be followed by the ATR-FTIR difference spectrum of the hydroxylated with respect the pristine hematite surfaces in Fig. 3b. The increase appears to more significantly affect the (11 $\overline{2}$ 0) orientation than the (1 $\overline{1}$ 0 0) and (0 0 0 1) orientations. This is a fundamental step toward surface reactivity because the hydroxylation process of the hematite plays an important role on anchoring starch molecules on the surface (Moreira et al., 2017).

Further investigation of the starch adsorbed on the hematite surfaces is explored by ATR-FTIR Difference measurements shown in Fig. 3c. The FTIR measurements are performed using 100 mg/L starch concentration since the amount adsorbed at 50 mg/L (shown in Fig. 1) is hardly detectable in our experimental setup. In Fig. 3c, the difference spectra for all surface orientations indicate changes related to the starch layers adsorbed. The changes are compared to gelatinized starch films (supporting material Figure S4) and are visible at approximately 1202 cm⁻¹ which is attributed to the O-H in-plane deformation coupled to the C—H deformation; 1162 cm⁻¹, which is attributed to the glycosidic linkage coupled with C—O stretching and O—H deformation ^{17,18}; 1094 cm⁻¹, which is attributed to the interaction of the —CO group with Fe (Subramanian and Natarajan, 1988); and near 1040 and 1005 cm⁻¹, which is associated with C—O related to the CO—H stretching vibration of starch (Tang et al., 2017); the band around 988 cm⁻¹ has been assigned to the vibration of C—O—C glycosidic bridge for starch (Pavlovic and Brandao, 2003; Nikonenko et al., 2000). These spectral band signatures are associated with several chemical changes related to the complexation of thin starch layers with surface hydroxyl groups (Weissenborn et al., 1995). Notably, the shifts in the band positions possibly reveal the consequences of the starch-hematite interface interaction, but the definite assignment is difficult since only a limited number of bands are clearly distinguishable. Nevertheless, the spectra in Fig. 3c with the slight increase in intensity of the 1162, 1094 and 988 cm⁻¹ bands suggest a larger amount of starch on the $(1 \ 1 \ \overline{2} \ 0)$ surface than the other two hematite orientations.

3.3. X-ray photoelectron spectroscopy measurements

To further clarify the chemical changes promoted on the starch-hematite interfaces, XPS analysis was carried out. XPS measurements were employed to investigate the surface chemical composition of the pristine surfaces and the surfaces after hydroxylation and starch adsorption. The survey spectra for the (1 1 $\overline{2}$ 0), (1 $\overline{1}$ 0 0) and (0 0 0 1) surfaces are shown in the supporting material in Fig. S5. All XPS surveys display the presence of the main surface chemical components, such as iron and oxygen, as well as small amounts of impurities (i. e., carbon, sodium, and titanium). After hydroxylation, we note a decrease in the peak intensity in the regions of Fe 2p and O 1s and an increase in the C 1s peak for all orientations.

In Figs. 4 and 5, high-resolution Fe 2p and C 1s XPS spectra, respectively, are shown for all surface orientations before and after hydroxylation and starch adsorption. The analysis of the high-resolution O 1s XPS spectra is shown for all surface orientations before, after hydroxylation and starch adsorption in the supporting material Fig. S6. The peak binding energies (BEs), full width at half maximum (FWHM) and percentage area (%) of each component obtained from the peak envelope fitting are summarized in supporting material Table 1. The Fe 2p peak envelope was analyzed considering that the intensity of each spin-orbit component can be fitted conveniently using three curves related to the different chemical environments of the surface cations (McIntyre and Zetaruk, 1977). However, this description is not accurate since the 2p states of transition metals are described by multiplet splitting (Gupta and Sen, 1975; Bagus et al., 2020). Yet, we have fitted the Fe 2p peak envelope with a relatively small set of components (C1, C2 and C3) to follow the peak asymmetry changes as function of the sample preparation. In this approach, we do not expect to describe the exact nature of multiple components but actually follow its asymmetry changes. Our simplified approach relies on the asymmetric shape of the Fe 2p peak for stoichiometric Fe₂O₃, which is partially converted into a symmetric shape as a function of the hydroxylation of the surface until it fully converts into an iron oxy-hydroxyl (McIntyre and Zetaruk, 1977; Grosvenor et al., 2004). In Fig. 4, the Fe 2p_{3/2} peak envelope was fitted using three components separated by \sim 1 eV. Following this procedure, the observed BEs are in good agreement with those reported for the Fe 2p_{3/2} region, ranging from ~710.3 to 712.9 eV. These BE values

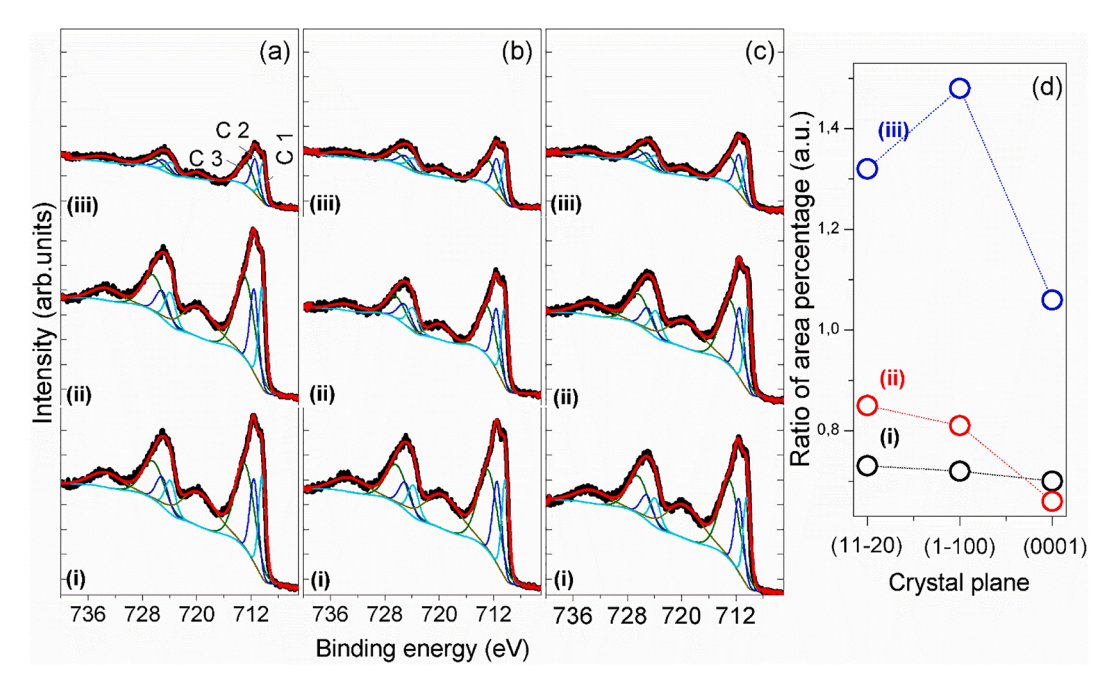


Fig. 4. High-resolution XPS spectra showing the original and deconvoluted Fe 2p peaks of hematite (a) (1 1 $\overline{2}$ 0), (b) (1 $\overline{1}$ 0 0) and (c) (0 0 0 1) surfaces: (i) pristine surface, (ii) after hydroxylation, and (iii) after 100 mg/L starch adsorption. The CPS of each spectrum was normalized to facilitate comparison. (d) Ratio of area percentage (%) of peak 2: peak 3 in Fe $2p_{3/2}$.

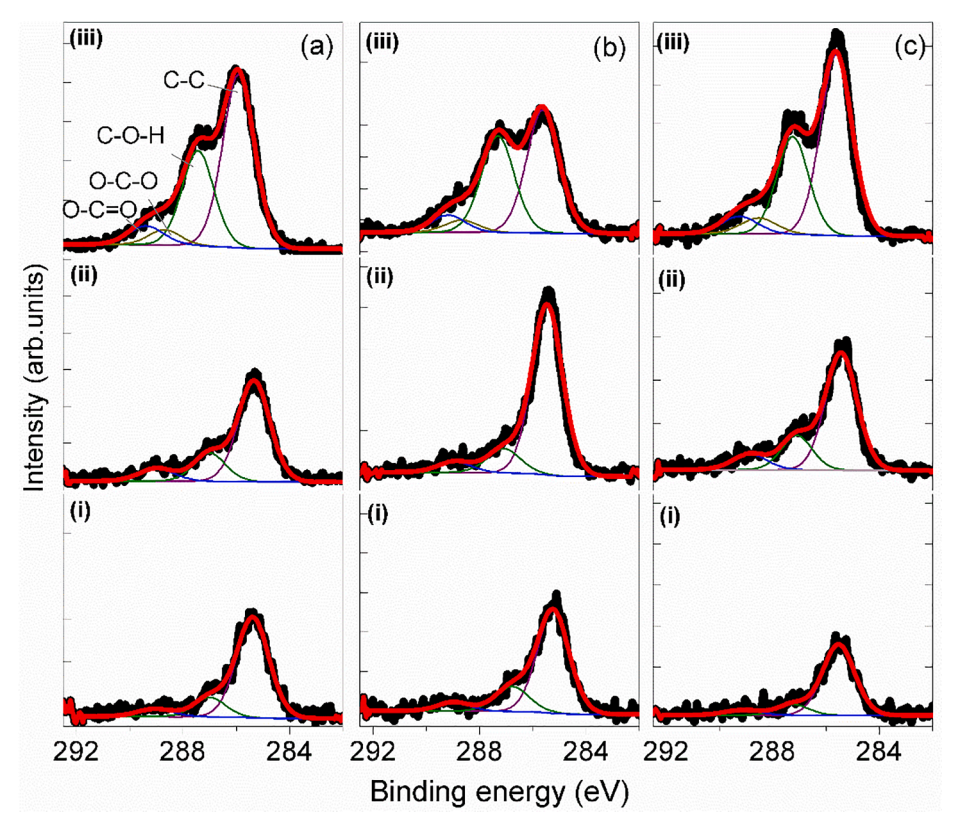


Fig. 5. High-resolution XPS spectra showing the original and deconvoluted C 1s peaks of hematite (a) $(1\ 1\ \overline{2}\ 0)$, (b) $(1\ \overline{1}\ 0\ 0)$ and (c) $(0\ 0\ 0\ 1)$ surfaces: (i) pristine surface, (ii) after hydroxylation, and (iii) after 100 mg/L starch adsorption. The CPS of each spectrum was normalized to facilitate comparison.

correspond to the Fe $^{3+}$ oxidation state in hematite. The corresponding satellite was observed at ~ 8 eV higher energy relative to the main Fe $2p_{3/2}$ component (McIntyre and Zetaruk, 1977). These general Fe 2p spectral features reveal that although the hematite surfaces are hydroxylated based on our FTIR measurements, their top most surface are

expected to preserve the hematite Fe_2O_3 character. Nevertheless, there are subtle changes for the pristine and hydroxylated surfaces when one compares the Fe 2p peak asymmetry based on the fitted components in Table 1 of the supporting material. First, despite the spectral similarities, we noted an increase in the relative intensity of component 2. The main

core peak was asymmetric to the high-energy side, but upon starch adsorption, most of this asymmetry is removed. These differences can be better observed by comparing the differences among the (1 1 $\overline{2}$ 0), (1 $\overline{1}$ 0 0) and (0 0 0 1) orientations. Notably, the satellite component was also affected, becoming less intense, as observed in our previous study 21 . The changes observed are related to the reduction in the coordination of iron surface atoms after pristine sample hydroxylation. The 2p peak features originated from surface atom-ligand interactions since the charge transfer occurring between the Fe 3d and O 2p unoccupied states in the valence band is strongly affected by the atom nearest-neighbor coordination (McIntyre and Zetaruk, 1977; Droubay and Chambers, 2001). These changes can be clearly observed in the spectra of all surfaces investigated.

Fig. 4d shows the comparative quantitative analysis of the area percentage ratio between peak components 2 and 3 for the Fe $2p_{3/2}$ peak envelope for the pristine, hydroxylated and starch-adsorbed surfaces. The intensity of the Fe $2p_{3/2}$ peak components was related to changes in the peak envelope asymmetry. Interestingly, the asymmetry appears to be more significant for the (1 1 $\overline{2}$ 0) and (1 $\overline{1}$ 0 0) surfaces than for the (0 0 0 1) surface. We note that the (0 0 0 1) surface is less affected by the hydroxylation and starch adsorption process, which suggests differences in the chemical interaction between the orientations.

Further analysis of the C 1s peak envelopes is shown in Fig. 5. The main C 1s peak envelope contains contributions from several components, including C-C/C-H at 284.5-285.5 eV, alcohol groups (C-OH) at 286.5-287.5 eV. glycosidic groups (O-C-O/C=O) at 287.9-288.6 eV and carboxylate groups (O-C=O) at 288.7-289.3 eV (Sun et al., 2014; Angellier et al., 2005; Lv et al., 2018). First, we note in Fig. 5i that even after the pretreatment of all single crystals under controlled conditions described in the Methods section, the C 1s peak persists on the pristine surface. For this reason, these carbon impurities may be related to residual carbon impurities present in the natural hematite single crystals. This residual carbon peak appears to increase after the hydroxylation treatment, as the relative intensity of alcohol groups slightly increased. Notably, the starch adsorbed onto hematite displayed notable differences in comparison to the hydroxylated surfaces. As expected, the components related to the starch molecules significantly increased and were identified as C-C/C-H, C-OH and O-C-O/C=O. These carboxylate groups are known to be related to the attachment of chemisorbed molecules on the FeO-OH and Fe-OH surface sites (Weissenborn et al., 1995; Moreira et al., 2017). The BEs of the alcohol and carboxylate groups were similar for all surface orientations but differed substantially from those observed for gelatinized starch films (Moreira et al., 2017). These changes suggest, in accordance with our previous study on hematite microparticulates, that starch molecules adsorb on the surfaces through C-OH and O-C=O groups. Notably, a comparative analysis indicates that the normalized relative amount of starch adsorbed is 1, 0.6 and 0.4 for the $(1 \ 1 \ \overline{2} \ 0)$, $(1 \ \overline{1} \ 0 \ 0)$ and $(0 \ 0 \ 0 \ 1)$ orientations, respectively. This estimation was performed by taking the peak area intensity ratio of C 1 s/Fe 2p of the starch-adsorbed surface divided by the same ratio obtained for the hydroxylated surface plane. The residual carbon contribution to the spectra occurs in the same manner for the hydroxylation and starch adsorption steps. Moreover, the AFM images of the samples prepared at 100 mg/L starch concentration (shown in Fig. 2) indicate that the substrate is extensively covered by starch (clean open patches are not visible compared to the images in Fig. 1), which enables the direct comparison of the peak ratio intensity changes. Thus, one can directly correlate the C 1 s increase for a given surface plane with the amount of adsorbed starch. Next, we normalized the relative increase in $(1 \ 1 \ \overline{2} \ 0)$ surface with respect the other surface orientations, assuming that the former is 1, as described in the Method section. Therefore, this finding agrees quite well with the AFM observations discussed in Figs. 1 and 2.

3.4. Adsorption mechanism proposal

In the next paragraphs, we attempt to understand the starch adsorption characteristics on each surface orientation based on both our own measurements and theoretical and experimental reports available in the literature. First, we consider that the differences in starch adsorption are related to hematite surface atom coordination (Ovcharenko et al., 2016). Several studies have shown that depending on the oxygen and hydrogen chemical potential, the topmost surface layer is decorated by either oxygen or triply coordinated iron atoms (Stumm, 1992; Lützenkirchen, 2015; Alvarez-Ramírez et al., 2004; Wang and Hellman, 2018; Wang, 1998). In any case, purely Fe-terminated surfaces are unlikely to be relevant under wet and highly alkaline conditions (Chatman et al., 2013; Boily, 2012; Chen et al., 2017; Liu et al., 2014; Ghose et al., 2010). In our analysis, we assumed that surface oxygen atoms are protonated under alkaline conditions (pH 10) and later, under starch adsorption conditions, are involved in the binding of the interfacial starch layer. Our general assumption on the surface structure is depicted in the tentative bulk-truncated models of each pristine surface plane in Fig. 6a ((1 1 $\overline{2}$ 0), (1 $\overline{1}$ 0 0) and (0 0 0 1) planes). The bond length values in Fig. 6 correspond to the bulk-hematite distances in the literature and may help the reader follow our reasoning on the calculated density of reactive sites²³. The yellow spheres represent iron, and the red spheres represent oxygen atoms. Hydrogen (in white) is considered to decorate all oxygen atoms but are not shown for clarity. In Fig. 6b, a glucopyranose molecular structural model is depicted with its functional groups, although their positions cannot be definitely determined in our experiments. The brown spheres represent carbon atoms, and again, most hydrogen atoms are omitted for clarity.

The depicted models in Fig. 6 agree with several earlier reports in which the oxygen-terminated surface was found to be stable (Chatman et al., 2015; Lützenkirchen, 2015). Obviously, under wet conditions, purely oxygen-terminated surfaces are unstable with respect to their hydroxylated counterparts (Tanwar, 2007). The hydroxylation process results in several changes in the surface structure related to the oxygeniron bond length and angle, charging and stability of each surface hydroxyl site (Chen et al., 2017). To support our simplified model, regarding the bonding length and angle, recent reports on hydroxylated hematite and goethite surfaces have shown that the interlayer Fe — Fe distance is the most affected, with only minor (oxygen-iron bond length changes from ~0.194 to 0.195–0.215 nm) structural relaxations expected for Fe — O bond, depending on their coordination and charge (Boily, 2012; Tanwar, 2007; Gittus et al., 2018).

Next, we analyzed a number of important differences among $(1 \ 1 \ \overline{2} \ 0), (1 \ \overline{1} \ 0 \ 0)$ and $(0 \ 0 \ 0 \ 1)$ that must be taken into account to understand their reactivity. Their termination consists of a stoichiometric Fe₂O₃ layer with an additional O topmost layer that completes the coordination shell of the upper Fe atoms. While all surface planes share similar features, the (0 0 0 1) plane contains only doubly coordinated oxygen atoms. Both the $(1\ 1\ \overline{2}\ 0)$ and $(1\ \overline{1}\ 0\ 0)$ planes are characterized by equally distributed numbers of (S) singly, (D) doubly and (T) triply coordinated oxygen atoms. From the surface termination models depicted in Fig. 6, we calculated the density of terminal lowcoordinate oxygen atoms, with values of 15 nm⁻² for (1 1 $\overline{2}$ 0), corresponding to 5 nm⁻² for each S-, D- and T-coordinated oxygen atom; 17.4 nm^{-2} for (1 $\overline{1}$ 0 0), corresponding to 5.8 nm^{-2} for each S-, D- and T-coordinated atom; and 13.6 nm⁻² for (0 0 0 1), with only D-coordinated oxygen atoms. The oxygen atoms on the pristine surface were expected to have formal valences of the S, D and T sites of -1.5, -1.0 and -0.5, respectively. Upon hydroxylation of the surface, protonation may result in S-, D-, and T-H surface hydroxyl groups with charges of -0.5, 0 and +0.5, respectively. The protonation of these sites is not equally favorable, and multisite protonation processes are fundamental to understanding their reactivity (Wang and Hellman, 2018; Chen et al., 2017; Ghose et al., 2010; Tanwar, 2007; Cudennec and Lecerf, 2006;

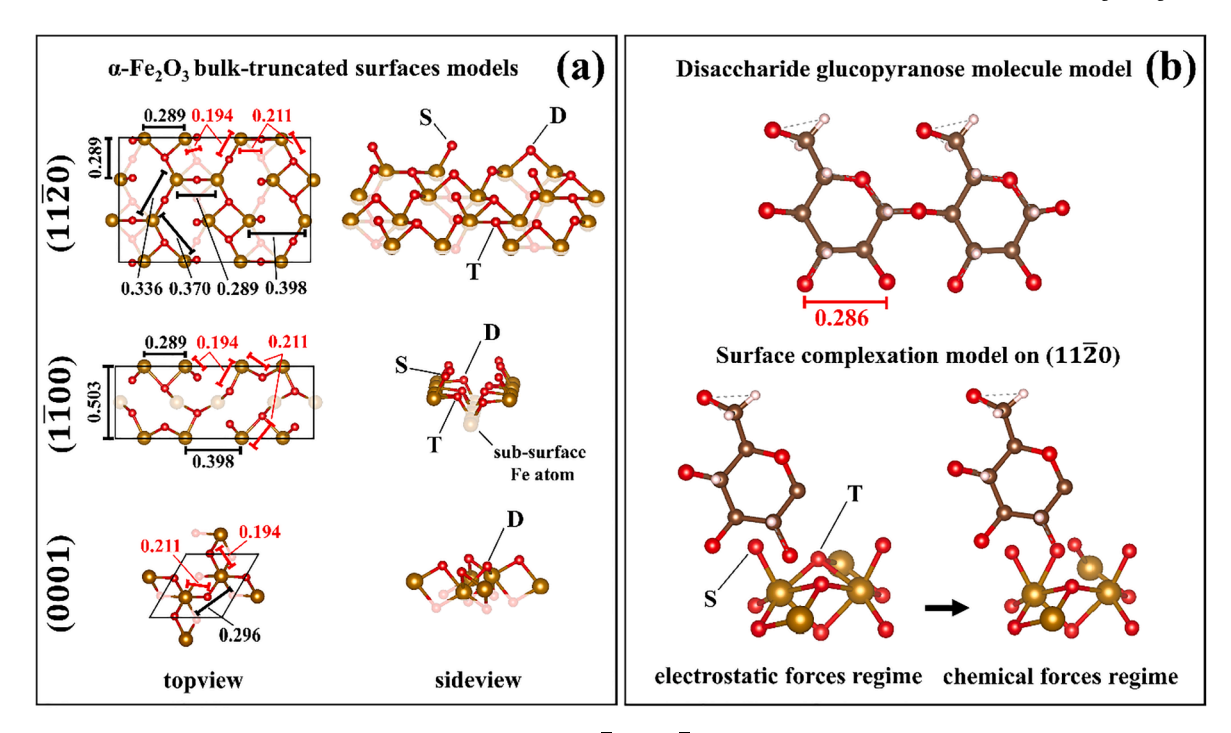


Fig. 6. Bulk-truncated models of each pristine surface plane in Fig. 6a (($1\ \bar{2}\ 0$), ($1\ \bar{1}\ 0$ 0) and (0 0 0 1) planes). The yellow spheres represent iron, the red spheres represent oxygen, the white spheres represent hydrogen, and the brown spheres represent carbon atoms. Notably, we assumed that the surface oxygen atoms are protonated at both the surface and molecule under alkaline conditions, but some protonation is omitted for clarity. (For interpretation of the references to colour in this figure legend, the reader is referred to the web version of this article.)

Ristić et al., 2007). In general, upon protonation of the D-H sites, the materials become nearly inert. On the other hand, S-H and T-H are constantly undergoing protonation and deprotonation in solution because of the instability of surface groups such $\label{eq:fe-oh} \text{Fe} - \text{OH}^{0.5-} + \text{H}^+ \rightarrow \text{Fe}^{0.5+} + \text{H}_2\text{O} \ \ \text{or} \ \ \text{Fe} - \text{OH}^{0.5-} + \text{OH}^- \rightarrow \text{Fe} - \text{O}^{1.5+} + \text{H}_2\text{O}$ for the former and $Fe_3 - OH^{0.5+} + H^+ \rightarrow Fe_3^{1.5+} + H_2O$ or $Fe_3 - OH^{0.5+} + OH^- \rightarrow Fe_3 - O^{0.5-} + H_2O$ for the latter. The straightforward analysis based solely on the one-step protonation process, however, could not reconcile the reactivity of a number of surface planes containing only doubly coordinated oxygen atoms (i.e., Al₂O₃ (0 0 0 1) or Fe₂O₃ (0001)) (Hiemstra and Van Riemsdijk, 1999; Barrón and Torrent, 1996; Venema et al., 1998; Hiemstra et al., 1989; Ruan et al., 2001; Hiemstra et al., 1989). Therefore, point defects or impurities on the surface may also act as promoters for S and T site formation and further reactivity. Our experimental results are obviously insensitive to the protons that might be associated with these surface oxygen atoms. However, the protonation state of the terminal oxygen is inferred considering the starch preferential adsorption on our selected hematite

Based on our measurements, a stronger starch interaction occurs in the following order: $(1 \ 1 \ \overline{2} \ 0) > (1 \ \overline{1} \ 0 \ 0) > (0 \ 0 \ 1)$. This behavior is related to the presence of highly reactive singly and triply coordinated surface atoms on the $(1 \ 1 \ \overline{2} \ 0)$ and $(1 \ \overline{1} \ 0 \ 0)$ surfaces. However, if one would consider only the surface density of low-coordinate oxygen atoms, a larger reactivity would be erroneously assigned to the $(1 \ \overline{1} \ 0 \ 0)$ surface plane. Thus, it is important now to compare the density of binding centers on each $(1\ 1\ \overline{2}\ 0)$ and $(1\ \overline{1}\ 0\ 0)$ surface plane. The mechanism of the starch-hematite interaction is related to surface complexation, where the organic molecules interact strongly with iron surface sites (Weissenborn et al., 1995; Subramanian and Natarajan, 1988). The number of available iron surface sites is otherwise difficult to directly determine but is expected to be consistent with the calculated iron density for the (11 $\overline{2}0$) and (1 $\overline{1}$ 0 0) surface planes, with values of 9.2 nm⁻² and 5.8 nm⁻², respectively. This comparison allows us to rationalize each surface reactivity as follows.

In previous studies using infrared spectroscopy, the behavior of starch adsorbed on hematite indicated the formation of chemical bonds between polysaccharides and surface iron atoms (Weissenborn et al., 1995; Moreira et al., 2017). Weissenborn et al supported the notion that surface complexation is related to hydroxyl groups attached to C-2 and C-3' (i.e., in the glucopyranose units shown in Fig. 6b) to form a complex with surface iron atoms. Following this mechanism, -OH groups on the starch molecule interact first via electrostatic forces (i.e., due to the dipole moment connected to the polarity of this functional group) to approach the hydroxylated surface at charged Fe-OH^{0.5-} and Fe₃ -O^{0.5-} species present on the hematite surfaces (Hiemstra et al., 1989; Hiemstra et al., 1989). The stabilization of these pairs was previously discussed by Hiemstra et al. We speculate that under strong alkaline conditions, the singly coordinated oxygen surface atom may also form short-lived Fe $-0^{1.5-}$ species on the surface. Note that on each $(1\ 1\ \overline{2}\ 0)$ and $(1\ \overline{1}\ 0\ 0)$ surface plane, singly coordinated oxygen shares the same iron surface atom with a nearby triply coordinated oxygen, which may potentially enhance the Fe⁺³ reactivity. This means that as the starch-OH group interacts with the Fe⁺³ site, the positive portion of the -OH group is placed close to the negative S-H site (Fe – OH^{0.5}–), while the negative portion is closer to the Fe⁺³ surface atom. Next, under alkaline conditions, deprotonation of the starch-OH group could lead to protonation of the S or T surface site. Structural relaxation of the T site related to the electrostatic repulsion of the relatively close negative portion of the starch-OH group favor the formation of a highly unstable T-H group (Fe₃ -OH^{0.5+}). This short-lived state could then become a Fe_3 – $OH^{0.5+}$ \rightarrow Fe – $OH^{0.5-}$ +Fe – $O_V^{1.5-}$ + $^{-0.5}$ OH -Fe -O - starch (O_V indicates an oxygen vacancy that, under alkaline conditions, is readily filled by a OH⁻ in solution). Alternatively, the reaction pathway of $Fe_3 - OH^{0.5+} \rightarrow Fe_2 - OH^{-0.5} + OFe - OFe$ starch would result in unlikely inert doubly coordinated $Fe_2 - O^{1.0-}$ sites (Hiemstra and Van Riemsdijk, 1999; Barrón and Torrent, 1996; Venema et al., 1998; Hiemstra et al., 1989; Hiemstra et al., 1989).

The key to understanding this mechanism is based on the surface structure analysis of each (1 $\overline{1}$ $\overline{2}$ 0) and (1 $\overline{1}$ 0 0) surface plane. The

reason for this conclusion is that the surface density of singly coordinated oxygen atoms on $(1 \ \overline{1} \ 0 \ 0)$ is larger than that on $(1 \ 1 \ \overline{2} \ 0)$. Therefore, singly coordinated site reactivity alone would not explain the larger amount of starch found on the $(11\overline{2}0)$ surface. However, more triply coordinated oxygen atoms are also observed on the $(1 \ \overline{1} \ 0 \ 0)$ surface. However, on the $(1 \ \overline{1} \ 0 \ 0)$ surface, one of the iron surface atoms bound to the triply coordinated oxygen is not contained on the topmost surface plane (i.e., it belongs to the subsurface iron atom, as indicated in Fig. 6a). This means that even though these iron atoms are prone to react, they are less likely to attach the starch-OH group due to geometrical reasons. Following this adsorption mechanism strictly, the further attachment of an adjunct intramolecular starch-OH group to nearby singly coordinated oxygen atoms results in a possible iron bidentate complex. This second step, however, decreases the relative density of highly reactive surface iron atoms. As a consequence, molecular packing on the surface and intermolecular interactions must be considered, but these aspects are out of the scope of the present study.

Thus, to the best of our knowledge, our data and analysis provide the first strong experimental evidence of starch adsorption dependence on hematite surface orientation. The outcome adds to well-established hydroxylation and surface complexation models, such as *multisite complexation* (MUSIC), and popular experimental methods, such as adsorption experiments, infrared spectroscopy and zeta potential measurements. Finally, we note that in the search for a better efficiency of the reverse flotation concentration process, further strategies must be explored to overcome rather inert surface planes, such as promoting an increase in mineral surface roughness and exposing their reactive surface plane.

4. Conclusions

To conclude, this study has demonstrated that starch complexation on hematite surfaces depends strongly on crystallographic and chemical properties. The experimental results indicate that the reactivity of these species follows the order $(1 \ 1 \ \overline{2} \ 0) > (1 \ \overline{1} \ 0 \ 0) > (0 \ 0 \ 1)$. Our results provide evidence of a multisite complexation mechanism, where both singly and triply coordinated oxygen surface sites react in pairs for the attachment of starch molecules. This mechanism must be rationalized not only based on the surface density of singly coordinated oxygen atoms but also in terms of the actual density of reactive iron sites on the surface. Based on these findings, we anticipate that the starch affinity to the $(1 \ 1 \ \overline{2} \ 0)$ surface plane is higher than that to the prevalent $(1 \ \overline{1} \ 0 \ 2)$ plane usually found in hematite nanostructures (Kraushofer, 2018). The reason for this finding is that for the latter, the surface density of iron atoms (7.3 nm⁻²) is smaller, and the singly coordinated oxygen atom has only one nearby triple-coordinated oxygen bound to one iron surface atom. More important, these fundamental aspects on the starch/hematite interactions may suggest that the fine tuning of hematite surface atoms bonding and density (i.e., employing preflotation chemical treatments) could potentially burst starch adsorption and, consequently, improve iron recovery in the concentration process. Finally, possible obvious shortcomings from our analysis arise as follows: (a) the exact Fe-O bond lengths; (b) molecular conformations under our experimental conditions; (c) the effects related to the Na⁺ ions in solution; and (d) molecular functional group electronegativity, particularly the role of the carboxylic groups. Therefore, although this study provides insight into an important topic for basic and applied research, more theoretical and experimental work is required to unambiguously understand the adsorption mechanism dependence on the surface crystallography on wet mineral interfaces.

Declaration of Competing Interest

The authors declare that they have no known competing financial interests or personal relationships that could have appeared to influence the work reported in this paper.

Acknowledgments

The authors acknowledge the Brazilian financial support from CAPES/ITV. This work was partially supported by CNPq and FAPERJ. F. Stavale thanks the Surface and Nanostructures Multiuser Lab at CBPF.

Appendix A. Supplementary data

Supplementary data to this article can be found online at https://doi.org/10.1016/j.mineng.2022.107429.

References

- Alvarez-Ramírez, F., Martínez-Magadán, J.M., Gomes, J.R.B., Illas, F., 2004. On the geometric structure of the (0 0 0 1) hematite surface. Surf. Sci. 558, 4–14.
- Angellier, H., Molina-Boisseau, S., Belgacem, M.N., Dufresne, A., 2005. Surface chemical modification of waxy maize starch nanocrystals. Langmuir 21 (6), 2425–2433
- Araujo, A.C., Viana, P.R.M., Peres, A.E.C., 2005. Reagents in iron ores flotation. Miner. Eng. 18, 219–224.
- Bagus, P.S., Nelin, C.J., Brundle, C.R., Lahiri, N., Ilton, E.S., Rosso, K.M., 2020. Analysis of the Fe 2p XPS for hematite α -Fe₂O₃: Consequences of covalent bonding and orbital splittings on multiplet splittings. J. Chem. Phys. 152, 014704.
- Barrón, V., Torrent, J., 1996. Surface hydroxyl configuration of various crystal faces of hematite and goethite. J. Colloid Interface Sci. 177, 407–410.
- Boily, J.F., 2012. Water structure and hydrogen bonding at goethite/water interfaces: Implications for proton affinities. J. Phys. Chem. C 116, 4714–4724.
- Cambier, P., 1986. Infrared study of goethites of varying crystallinity and particle size: I. Interpretation of OH and lattice vibration frequencies. Clay Miner. 21, 191–200.
- Chatman, S., Zarzycki, P., Rosso, K.M., 2013. Surface potentials of (001), (012), (113) hematite (α-Fe2O3) crystal faces in aqueous solution. Phys. Chem. Chem. Phys. 15, 13911–13921.
- Chatman, S., Zarzycki, P., Rosso, K.M., 2015. Spontaneous water oxidation at hematite (α-Fe2O3) crystal faces. ACS Appl. Mater. Interfaces 7, 1550–1559.
- Chen, Y., Bylaska, E.J., Weare, J.H., 2017. Weakly bound water structure, bond valence saturation and water dynamics at the goethite (100) surface/aqueous interface: Ab initio dynamical simulations. Geochem. Trans. 18, 1–14.
- Chernyshova, I.V., Hochella, M.F., Madden, A.S., 2007. Size-dependent structural transformations of hematite nanoparticles. 1. Phase transition. Phys. Chem. Chem. Phys. 9, 1736–1750.
- Cornell, R.M., Schwertmann, U., 2004. Introduction to the Iron Oxides. The Iron Oxides. Cudennec, Y., Lecerf, A., 2006. The transformation of ferrihydrite into goethite or hematite, revisited. J. Solid State Chem. 179 (3), 716–722.
- Droubay, T., Chambers, S.A., 2001. Surface-sensitive Fe2p photoemission spectra for α -Fe2O3(0001): The influence of symmetry and crystal-field strength. Phys. Rev. B 64, 205414.
- Farmer, V.C., 1968. Infrared Spectroscopy Studies in Clay Mineral. Clay Miner. 7, 373–387.
- Fateley, W.G., McDevitt, N.T., Bentley, F.F., 1971. Infrared and Raman Selection Rules for Lattice Vibrations: The Correlation Method. Appl. Spectrosc. 25, 155–173.
- Figuerola, A., Di Corato, R., Manna, L., Pellegrino, T., 2010. From iron oxide nanoparticles towards advanced iron-based inorganic materials designed for biomedical applications. Pharmacol. Res. 62, 126–143.
- Filippov, L.O., Severov, V.V., Filippova, I.V., 2014. An overview of the beneficiation of iron ores via reverse cationic flotation. Int. J. Miner. Process. 127, 62–69.
- Fischer, W.R., Schwertmann, U., 1975. The formation of hematite from amorphous iron (III)hydroxide. Clays Clay Miner. 23, 33–37.
- Ghose, S.K., Waychunas, G.A., Trainor, T.P., Eng, P.J., 2010. Hydrated goethite (α-FeOOH) (1 0 0) interface structure: Ordered water and surface functional groups. Geochim. Cosmochim. Acta 74, 1943–1953.
- Gittus, O.R., Von Rudorff, G.F., Rosso, K.M., Blumberger, J., 2018. Acidity Constants of the Hematite-Liquid Water Interface from Ab Initio Molecular Dynamics. J. Phys. Chem. Lett. 9, 5574–5582.
- Gotić, M., Musić, S., 2007. Mössbauer, FT-IR and FE SEM investigation of iron oxides precipitated from FeSO4 solutions. J. Mol. Struct. 834-836, 445-453.
- Grosvenor, A.P., Kobe, B.A., Biesinger, M.C., McIntyre, N.S., 2004. Investigation of multiplet splitting of Fe 2p XPS spectra and bonding in iron compounds. Surf. Interface Anal. 36 (12), 1564–1574.
- Gupta, R.P., Sen, S.K., 1975. Calculation of multiplet structure of core p-vacancy levels.

 II. Phys. Rev. B 12, 15–19.
- Hiemstra, T., De Wit, J., C., M. & Riemsdijk, W.H.V., 1989. Multisite proton adsorption modeling at the solid/solution interface of (hydr)oxides: A new approach: II. Application to various important (hydr)oxides. J. Coll. Interface Sci. 133, 105–117.
- Hiemstra, T., Riemsdijk, W. H. V. & B. G., 1989. Multisite proton adsorption modeling at the solid/solution interface of (hydr)oxides: A new approach. J. Coll. Interface Sci. 133, 91–104.
- Hiemstra, T., Van Riemsdijk, W.H., 1999. Effect of different crystal faces on experimental interaction force and aggregation of hematite. Langmuir 15 (23), 8045–8051.
- Hofmeister, A.M., 1993. IR reflectance spectra of natural ilmenite: comparison with isostructural compounds and calculation of thermodynamic properties. Eur. J. Mineral. 5 (2), 281–296.

- Humez, N., Prost, R., 1999. A new experimental approach to study the longterm behaviour of solidified/stabilized wastes. Chem. Speciat. Bioavailab. 11, 1–24.
- Kim, J.Y., et al., 2013. Single-crystalline, wormlike hematite photoanodes for efficient solar water splitting. Sci. Rep. 3, 1–8.
- Kraushofer, F., et al., 2018. Atomic-Scale Structure of the Hematite α -Fe2O3(11–02) 'r-Cut' Surface. J. Phys. Chem. C 122, 1657–1669.
- Laskowski, J.S., Liu, Q., O'Connor, C.T., 2007. Current understanding of the mechanism of polysaccharide adsorption at the mineral/aqueous solution interface. Int. J. Miner. Process. 84, 59–68.
- Leal Filho, L.S., Seidl, P.R., Correia, J.C.G., Cerqueira, L.C.K., 2000. Molecular modelling of reagents for flotation processes. Miner. Eng. 13, 1495–1503.
- Liu, H., Chen, T., Frost, R.L., 2014. An overview of the role of goethite surfaces in the environment. Chemosphere 103, 1–11.
- Liu, Q., Zhang, Y., Laskowski, J.S., 2000. The adsorption of polysaccharides onto mineral surfaces: An acid/base interaction. Int. J. Miner. Process. 60, 229–245.
- Lützenkirchen, J., et al., 2015. Structure-charge relationship The case of hematite (001). Faraday Discuss. 180, 55–79.
- Lv, S., Zhang, Y., Gu, J., Tan, H., 2018. Soil burial-induced chemical and thermal changes in starch/poly (lactic acid) composites. Int. J. Biol. Macromol. 113, 338–344.
- McIntyre, N.S., Zetaruk, D.G., 1977. X-ray Photoelectron Spectroscopic Studies of Iron Oxides. Anal. Chem. 49, 1521–1529.
- Mhonde, N.P., Wiese, J.G., McFadzean, B., 2017. Comparison of collector performance for a South African and a Brazilian iron ore considering mineralogical characteristics. Miner. Eng. 113, 55–67.
- Moreira, G.F., Peçanha, E.R., Monte, M.B.M., Leal Filho, L.S., Stavale, F., 2017. XPS study on the mechanism of starch-hematite surface chemical complexation. Miner. Eng. 110, 96–103.
- Morterra, C., Chiorino, A., Borello, E., 1984. An IR spectroscopic characterization of α -FeOOH (Goethite). Mater. Chem. Phys. 10, 119–138.
- Nikonenko, N.A., Buslov, D.K., Sushko, N.I., Zhbankov, R.G., 2000. Investigation of stretching vibrations of glycosidic linkages in disaccharides and polysaccarides with use of IR spectra deconvolution. Biopolymers (Biospectroscopy) 57 (4), 257–262.
- Onari, S., Arai, T., Kudo, K., 1977. Infrared lattice vibrations and dielectric dispersion in α -Fe2O3. Phys. Rev. B 16, 1717–1721.
- Ovcharenko, R., Voloshina, E., Sauer, J., 2016. Water adsorption and O-defect formation on Fe2O3(0001) surfaces. Phys. Chem. Chem. Phys. 18, 25560–25568.
- Patra, A.K., Kundu, S.K., Bhaumik, A., Kim, D., 2016. Morphology evolution of singlecrystalline hematite nanocrystals: Magnetically recoverable nanocatalysts for enhanced facet-driven photoredox activity. Nanoscale 8 (1), 365–377.
- Pavlovic, S., Brandao, P.R.G., 2003. Adsorption of starch, amylose, amylopectin and glucose monomer and their effect on the flotation of hematite and quartz. Miner. Eng. 16, 1117–1122.
- Pham, A.L.T., Lee, C., Doyle, F.M., Sedlak, D.L., 2009. A silica-supported iron oxide catalyst capable of activating hydrogen peroxide at neutral pH values. Environ. Sci. Technol. 43, 8930–8935.
- Prasad, P.S.R., Shiva Prasad, K., Krishna Chaitanya, V., Babu, E.V.S.S.K., Sreedhar, B., Ramana Murthy, S., 2006. In situ FTIR study on the dehydration of natural goethite. J. Asian Earth Sci. 27 (4), 503–511.
- Ravishankar, S.A., Pradip, Khosla, N.K., 1995. Selective flocculation of iron oxide from its synthetic mixtures with clays: a comparison of polyacrylic acid and starch polymers. Int. J. Miner. Process. 43 (3-4), 235–247.

- Rendon, J.L., Serna, C.J., 1981. IR spectra of powder hematite: effects of particle size and shape. Clay Miner. 16, 375–382.
- Ristić, M., De Grave, E., Musić, S., Popović, S., Orehovec, Z., 2007. Transformation of low crystalline ferrihydrite to α-Fe2O3 in the solid state. J. Mol. Struct. 834-836,
- Ruan, H.D., Frost, R.L., Kloprogge, J.T., 2001. The behavior of hydroxyl units of synthetic goethite and its dehydroxylated product hematite. Spectrochim. Acta - Part A Mol. Biomol. Spectrosc. 57 (13), 2575–2586.
- Shrimali, K., et al., 2018. The nature of hematite depression with corn starch in the reverse flotation of iron ore. J. Colloid Interface Sci. 524, 337–349.
- Silva, C.E., Silva, L.P., Edwards, H.G.M., De Oliveira, L.F.C., 2006. Diffuse reflection FTIR spectral database of dyes and pigments. Anal. Bioanal. Chem. 386, 2183–2191.
- Stumm, W., 1992. Chemistry of the Interface Processes at the Mineral-Water. New York. Subramanian, S., Natarajan, K.A., 1988. Some studies on the adsorption behaviour of an oxidised starch onto hematite. Miner. Eng. 1, 241–254.
- Sun, W., Li, Q., Zhou, F., Zhao, H., Zhao, M., 2014. Surface characterization of oxidized myofibrils using X-ray photoelectron spectroscopy and scanning electron microscopy. J. Agric. Food Chem. 62, 7507–7514.
- Tang, M., Liu, Q.i., 2012. The acidity of caustic digested starch and its role in starch adsorption on mineral surfaces. Int. J. Miner. Process. 112-113, 94–100.
- Tang, M., Wen, S., Tong, X., 2017. Caustic-digested starch and its adsorption on hematite. Physicochem. Probl. Miner. Process. 53, 69–81.
- Tanwar, K.S., et al., 2007. Surface diffraction study of the hydrated hematite (1–102) surface. Surf. Sci. 601, 460–474.
- Taylor, S.D., Kovarik, L., Cliff, J.B., Rosso, K.M., 2019. Facet-selective adsorption of Fe (II) on hematite visualized by nanoscale secondary ion mass spectrometry. Environ. Sci.: Nano 6, 2429.
- Turrer, H.D.G., Peres, A.E.C., 2010. Investigation on alternative depressants for iron ore flotation. Miner. Eng. 23, 1066–1069.
- Venema, P., Hiemstra, T., Weidler, P.G., Van Riemsdijk, W.H., 1998. Intrinsic proton affinity of reactive surface groups of metal (hydr)oxides: Application to iron (hydr) oxides. J. Colloid Interface Sci. 198, 282–295.
- Verdonck, L., Hoste, S., Roelandt, F.F., Van Der Kelen, G.P., 1982. Normal coordinate analysis of α -FeOOH a molecular approach. J. Mol. Struct. 79, 273–279.
- Wang, X.G., et al., 1998. The hematite (α-Fe2O3) (0001) surface: Evidence for domains of distinct chemistry. Phys. Rev. Lett. 81, 1038–1041.
- Wang, R.B., Hellman, A., 2018. Surface terminations of hematite (α-Fe2O3) exposed to oxygen, hydrogen, or water: Dependence on the density functional theory methodology. J. Phys. Condens. Matter 30 (27), 275002. https://doi.org/10.1088/ 1361-648X/aac743.
- Wang, Y., Muramatsu, A., Sugimoto, T., 1998. FTIR analysis of well-defined α -Fe2O3 particles. Colloids Surf. A Physicochem Eng. Asp. 134 (3), 281–297.
- Weissenborn, P.K., Warren, L.J., Dunn, J.G., 1995. Selective flocculation of ultrafine iron ore. 1. Mechanism of adsorption of starch onto hematite. Coll. Surf. A Physocochem. Eng. Asp. 99, 11–27.
- Xia, L., Zhong, H., Liu, G., Wang, S., 2009. Utilization of soluble starch as a depressant for the reverse flotation of diaspore from kaolinite. Miner. Eng. 22, 560–565.
- Li Yan, Tingshan Chan, Chuanyong Jing, 2020. Arsenic adsorption on hematite facets: spectroscopy and DFT study. Environ. Sci.: Nano, 7, 3927.